PCCP

Accepted Manuscript

ROYAL SOCIETY OF CHEMISTRY

www.rsc.org/pccp

Direct Observation of Breaking the Intramolecular H-bond, Slowing Down the Proton Motion and Tuning its Mechanism in an HBO Derivative

Noemí Alarcos, ‡[1] Mario Gutierrez, ‡[1] Marta Liras,[2] Félix Sánchez,[2] Miquel Moreno[3] and Abderrazzak Douhal[1*]

[1]Departamento de Química Física, Facultad de Ciencias Ambientales y Bioquímica, and INAMOL, Universidad de Castilla-La Mancha, Avenida Carlos III, S.N., 45071 Toledo, Spain.

[2] Instituto de Química Orgánica General, IQOG-CSIC, Juan de la Cierva, 3, 28006 Madrid, Spain

[3] Departament de Química, Universitat Autónoma de Barcelona, Bellaterra, 08193 Barcelona, Spain.

‡ Equal contributions

*Corresponding author at Universidad de Castilla-La Mancha.

Tel.: +34 925 265717; E-mail address: abderrazzak.douhal@uclm.es

Abstract

We report on the spectroscopic and photodynamical behaviours of 5-amino-2-(2'-hydroxyphenyl)benzoxazole (5A-HBO) in different solutions. The dye exhibits an ultrafast ICT reaction (<50 fs) (comparable to that observed for its methylated derivative, 5A-MBO), in agreement with the results of TD-DFT theoretical calculations (gas phase). Depending on the used solvent, the ICT reaction can be followed by a reversible/irreversible excited-state intramolecular proton transfer (ESIPT) reaction or by breaking of the intramolecular hydrogen bond (IHB). 5A-HBO in n-heptane solution exhibits an irreversible and slow (20 ps) ESIPT reaction, while that of the parent compound, HBO, takes place in less than 150 fs. Compared to excited HBO behaviour, the theoretical calculations for 5A-HBO suggest a higher energy barrier (~4 kcal/mol) between the relaxed enol and keto tautomers, in addition to a less stabilization of the latter, which is in agreement with the experiments in n-heptane. On the other hand, in dichloromethane, after the ICT reaction a subsequent and reversible proton motion occurs in an extraordinary slower regime (ns-time scale). No isotopic effect (OH/OD exchange) was observed in this solvent reflecting that the reversible ESIPT reaction evolves along the IHB and solvent coordinates. Using tetrahydrofurane and acetonitrile, we observed a breaking of the IHB due to sepcific intermolecular interactions with the solvent molecules. This leads to the formation of open-enol forms which experience an ICT reaction as it happens in the 5A-MBO. These results bring new findings in the coupled ICT and ESIPT reactions. The photobehaviour of this new dye remarkably changes with the solvent nature, opening the window for further research, and possible applications in sensing polarity or H-bonding of media like of the biological ones.

Keywords:

Charge transfer, proton transfer, benzoxazole, ultrafast dynamics, femtochemistry.

1. Introduction

Organic molecules showing excited state intramolecular proton transfer (ESIPT) reactions have been investigated extensively because of their potential applications as well as the fundamental importance of the proton transfer in chemistry and biology.[1-15] The modification of the dye structure by introducing a functional group has been used for the generation of white-light-emitting materials[16, 17] tunneling laser actions[2, 18] and multicolor molecular probes for biological applications.[14, 19, 20] Such modification can produce changes in the spectroscopy and dynamics due to the involvement of intramolecular charge transfer (ICT), that happens along with the ESIPT. Both reactions can be coupled and different stepwise mechanisms have been proposed.[21-30]

A well-known proton-transfer dye; 2-(2'-hydroxyphenyl)benzoxazole (HBO), in which the ESIPT reaction takes place in ~150 fs,[31] exhibits remarkable changes in the ESIPT reaction and related spectroscopy when an acceptor or a donor group is in its molecular framework. In this sense, HBO derivatives containing electron-withdrawing groups in the 6-position of the benzoxazole ring such as 2-[[2-(2-hydroxyphenyl)benzo[d]oxazol-6-yl]methylene]malononitrile (diCN-HBO),[26] heptan-3-yl 2-cyano-3-(2-(2-hydroxyphenyl)benzo[d]oxazol-6-yl)propanoate (HBOCE)[28, 29] and 2-((2-(2-hydroxyphenyl)benzo[d]oxazol-6-yl)methylene)malononitrile (HBODC)[28] have been shown to exhibit ESIPT reactions followed by an ICT one. These molecules present different behaviours; while for diCN-HBO the ESIPT reaction is directly coupled with solvent polarization (changing the ESIPT rate constant from 1.1 ps in cyclohexane to 0.3 ps in acetonitrile (ACN)),[26] for HBOCE the reaction shows a bimodal behaviour with time constants of 250 fs and 1.2 ps due to the conformational heterogeneity in the ground state.[29] On the other hand, in an HBO derivative containing an electron-donating group in the same position as in HBOCE; 6-amino-2-(2'-hydroxyphenyl)benzoxazole (6A-HBO), the ICT reaction takes place prior to the ESIPT one.[24, 32, 33] In this case, the ESIPT reaction is even slower than the previous examples, with time constants from 1 to 35 ps (in n-heptane and methanol (MeOH) solutions, respectively).[32] Moreover, in H-bonding acceptor solvents like ACN and tetrahydrofurane (THF), this reaction is reversible and presents time constants up to hundreds of picoseconds,[24] while for solvent with strong H-bonding acceptor abilities (N,N-dimethylformamide, DMF) the proton motion does not take place and only the

open-enol species are observed.[33] Clearly, the substituent character (electron donor or acceptor) and the nature of the used solvent change the ESIPT reaction dynamics, which is coupled to the ICT one. To further explore the effect of the position of the amino group in the HBO moiety, we here report on theoretical calculations and photodynamical behaviour of 5-amino-2-(2'-hydroxyphenyl)benzoxazole (5A-HBO) and its methylated derivative (5-amino-2-(2'-methoxyphenyl)benzoxazole, 5A-MBO) in different solvents. For both molecules we find that an ultrafast ICT reaction occurs below the system resolution (<50 fs), and it is followed by the solvent relaxation (0.7-1.1 ps). 5A-HBO in n-heptane exhibits a subsequently abnormally slow (20 ps) and irreversible ESIPT reaction, while in DCM it is reversible with time constants of forward and backward proton motion in the ns-regime. In ACN and THF solutions, the excited 5A-HBO presents the breaking of the intramolecular H-bond and the formation of the intermolecular one with the solvent molecules. We compare and discuss the results with those obtained using the methylated derivatives; 5A-MBO (Scheme 1), a molecule which exhibits an ICT, but cannot undergoes an ESIPT reaction. Comparing the results described here with those obtained for 6A-HBO,[24, 32, 33] the reported here for 5A-HBO show that the position of the amino group strongly affects the ICT and ESIPT dynamics. The ICT reaction occurs faster than that observed for 6A-HBO, while that of ESIPT is disfavored due to intermolecular interaction with solvent molecules. We believe that our findings are giving new knowledge which was not available, and could be used for better design of proton transfer dyes for sensing and related fields.

2. Experimental Section

Calculations have been done on the HBO and 5A-HBO molecular systems in gas phase. Geometries have been optimized at the DFT level using the hybrid CAM-B3LYP functional in order to prevent failures when dealing with excited states with a noticeable degree of intramolecular charge transfer.[34] The extended 6-31G(d,p) basis set has been used in all the calculations.[35, 36] The ten lowest singlet excited states have been then calculated at the ground-state minimum energy geometry (Franck-Condon approximation) using the TD-DFT level and the same CAM-B3LYP functional. The minimum energy structures (enol and keto) in the lowest singlet excited state have been then localized by full minimization at the same level of calculation. Finally the

transition states in the excited states have been approximately located by means of a reaction coordinate calculation. All the calculations have been carried out with the GAUSSIAN09 suite of programs.[37]

The synthesis, purification and characterization of 5-amino-2-(2-methoxyphenyl)benzoxazole (5A-MBO) and 5-amino-2-(2-hydroxyphenyl)benzoxazole (5A-HBO) are described in our previous report.[33] The deuterated compound (5A-DBO) was obtained heating 5A-HBO in deuterated methanol and evaporating the solvent.

The used solvents (anhydrous): n-heptane (99%), dichloromethane (DCM, 99.9%), acetonitrile (ACN, 99.8%) and tetrahydrofurane (THF, 99.9%) were purchased from Sigma-Aldrich. The deuterated solvent: dichloromethane (DCM-d_2, 99.9%) was from Sigma-Aldrich. All the solvents were used as received.

The steady-state UV-visible absorption and fluorescence spectra have been recorded using JASCO V-670 and FluoroMax-4 (Jobin-Yvon) spectrophotometers, respectively. Fluorescence quantum yields were measured using Quinine Sulfate in a 0.1 N H_2SO_4 solution as a reference ($\varphi = 0.51$ at 293 K).[38]

Pico-nanosecond emission decays were measured using a time-correlated single photon counting (TCSPC) system.[39] The sample was excited by a 40-ps pulsed diode laser centered at 371 nm (<5 mW, 40 MHz repetition rate). The emission signal was collected at the magic angle and the instrument response function (IRF) was ~70 ps. The IRF of the system has been measured using a standard LUDOX (Sigma-Aldrich) solution in 1 cm cell. The decays were deconvoluted and fitted to a single or multiexponential function using the FLUOFIT package (PicoQuant) allowing single and global fits. The quality of the fit was estimated by χ^2 which was always below 1.2, and the distribution of the residues. The time-resolved emission spectra (TRES) were constructed from the single-wavelength measurements, and the zero time spectrum was taken as the one obtained at the intensity half-maximum corresponding to the rise of the excitation pulse. All experiments were done at 293 K.

The femtosecond (fs) emission transients have been collected using the fluorescence up-conversion technique. The system consists of a femtosecond Ti:sapphire oscillator MaiTai HP (Spectra Physics) coupled to a second harmonic generation and up-conversion setups.[40] The oscillator pulses (90 fs, 250 mW, 80 MHz) were centered at 720 nm and doubled in an optical setup through a 0.5-mm BBO crystal to generate a pumping beam at 360 nm (~ 0.1 nJ/pulse). The polarization of the latter was set to magic angle in respect to the fundamental beam. The sample has been placed

in 1-mm thick rotating cell. The fluorescence was focused with reflective optics into a 1-mm BBO crystal and gated with the fundamental fs-beam. The IRF of the full setup (measured as a Raman signal of pure solvent) was ~220 fs. To analyze the decays, a multiexponential function convoluted with the IRF was used to fit the experimental transients. All experiments were performed at 293 K.

3. Results and Discussion

3.1 Theoretical part

3.1.1 Gas phase

The results of the TD-DFT calculations show that only one minimum energy structure is present in the ground state (S_0) of both HBO and 5A-HBO molecules with the hydrogen bonded to the phenol moiety (syn-enol structure, Scheme 1). The calculation of the ten lowest singlet excited electronic states at this geometry (vertical excitation) reveals that in both systems the lowest excited state mostly comes from the HOMO-LUMO $\pi\pi^*$ electronic excitation. Figure 1 depicts the shape of these two orbitals for both systems of different structures. At S_0, the electronic density of the HOMO of HBO is mainly localized in the phenol part, while that of 5A-HBO it is in the benzoxazole one. However, at S_1, after of a vertical excitation, the electronic density is redistributed over all the molecular structure. Thus, the electronic density goes in opposite direction for both molecules since for HBO it migrates from the phenol part to the benzoxazole one, while for 5A-HBO it is from benzoxazole moiety to the phenol one. These differences could explain the different observed behaviours for both molecules, as we see below.

On the other hand, the energy of the lowest singlet excited electronic states (in gas phase) allows for a theoretical prediction of the absorption spectra of these species. For HBO the lowest two electronic transitions from the ground state are permitted (they have a non-negligible value of the oscillator strength) and predicted to appear at 286 and 250 nm. In the 5A-HBO system the second singlet excited state is optically inactive (very small value of the oscillator strength) but the transition to the third one, not far in energy, is allowed. Thus, two bands are theoretically predicted for the absorption spectra of this molecule now at 295 and 241 nm. These values are in agreement with the experimental absorption spectra (~340 and ~270 nm, respectively) as the differences

between the experimental results and the theoretical calculations fall within the expected error of the TD-DFT methodology (0.5 eV).

Figure 2 depicts the whole energy landscape obtained for both HBO and 5A-HBO in gas phase for both the ground (S_0) and first singlet (S_1) excited electronic states. At S_1, two minima were localized with the hydrogen atom (OH) either bonded to the phenol (enol) or the benzoxazole (keto) region of the molecule. Both minima can be connected through an excited-state intramolecular-transfer (ESIPT) process. In the parent HBO, molecule the excited keto form is clearly the more stable one (by more than 3 kcal/mol). There is also a very small energy barrier (~1.5 kcal/mol) for the ESIPT reaction, which can take place from the optimized relaxed excited enol form (E*). However the vertical (Franck-Condon) transition, indicated by a vertical red arrow in Figure 2, puts the excited system above this energy barrier so that ESIPT may proceed in an ultrafast way following the electronic excitation. Very interestingly, for 5A-HBO the two tautomers (relaxed E* and K* structures) forms are almost degenerate (the keto remains as the most stable but by 0.3 kcal/mol). Moreover, the energy barrier (4 kcal/mol) is higher than the one found for HBO (1.4 kcal/mol) though the Franck-Condon transition still gives the system enough energy to overcome the barrier. Finally for both keto structures at S_0, the reverse proton transfer reaction is expected to proceed without energy barrier to recover the enol populations.

Table S1 contains the Cartesian coordinates of the relevant geometries calculated for the different HBO and 5A-HBO structures. From these data the geometry of the molecules can be generated.

3.1.2 Mulliken charges and dipole moments

Another point of interest to be theoretically analyzed is the amount of charge transfer that takes place along the whole photochemical process at S_1. Table 1 gives the total Mulliken charges of the phenol side for HBO and 5A-HBO at the structures along the process. For the parent HBO, it is noted that the electronic excitation without geometry optimization involves an electronic redistribution from the phenol moiety to the benzoxazole ring as its charge increases from 0.080 to 0.207. The geometry relaxation upon electronic excitation (E*(FC) → E*) does not produce a noticeable change in the total charge of the phenol part but the following ESIPT leaves the phenol with a large amount of negative charge (-0.39 au) (Table 1). The difference of charge

between the E* and K* tautomers implies that the transferred hydrogen atom has a positive charge of 0.590 au (in general terms, the particle that is transferred has a 59% character of a proton). For 5A-HBO the electronic excitation implies a negligible electronic redistribution between the enol and the benzoxazole part of the molecule. However, unlike HBO, a charge migration (0.09 au) from the amino-benzoxazol moiety to the phenol one, between E*(FC) and relaxed E*, is observed. This value is ten times longer than the observed in HBO (≈0.009). The final hydrogen atom transfer in 5A-HBO (relaxed E* → K*) results in a 0.4 au. The small charge transfer character (9 %) (E* (FC) → E*) is not quite agree with what we observe experimentally (see below). However the charge analysis performed so far just takes into account a very restricted charge-transfer process between two specific parts of the molecule. A more accurate picture of the whole charge redistribution can be obtained if we calculate the variation of the dipole moment along the specific processes. Table 3 gives the dipole moment variation (Δμ) (in gas phase) for HBO and 5A-HBO due to three events: Electronic excitation (E → E*(FC)), geometry relaxation of the enol in S_1 (E*(FC) → E*) and ESIPT (E* → K*). In the E → E*(FC) transition, the Δμ for both molecules is similar (2.2 and 1.8 D for HBO and 5A-HBO, respectively). However, in the (E*(FC) → E*) transition, the Δμ for 5A-HBO (3.7 D) is higher than for HBO (0.3 D), suggesting an ICT reaction in the former. Finally, in the (E* → K*) transition this variation is high for both molecules although still is higher for 5A-HBO (4.1 D) than for HBO (2.8 D). These results demonstrate that the presence of a donating group (-NH_2) in the molecular frame produces an increase in the charge density which is reflected in the dipole moment.

3.2 Steady-state Absorption and Fluorescence Spectra

The steady-state UV-visible absorption and emission behaviour of 5A-HBO and its methylated derivative 5A-MBO in n-heptane, DCM, THF and ACN solutions were studied. Figure 3 displays the spectra of both molecules in these solvents. For both dyes, the $S_0 \rightarrow S_2$ (~270 nm) and $S_0 \rightarrow S_1$ (330-346 nm) absorption spectra are similar for all the used solvent, showing a vibrational structure for the higher transition while it is not clear or absent for the lowest one. These transitions are in agreement with the observed in the theoretical part where we predicted two bands at 241 and 295, taking into account

the expected error of the TD-DFT methodology (0.5 eV). Moreover, the 5A-HBO $S_0 \rightarrow S_1$ absorption spectra shows a small red-shift (~ 900 cm^{-1}) in their maxima when compared to those of 5A-MBO, indicating the stabilization in the first one due to the presence of an intramolecular H-bond (IHB, Scheme 1). The molar extinction coefficients of 5A-MBO (ε_{DCM} (340 nm) = 1.83 x 10^4 M^{-1} cm^{-1}) and 5A-HBO (ε_{DCM} (340 nm) = 0.58 x 10^4 M^{-1} cm^{-1}) are similar and high indicating that they are of (π,π*) nature. Moreover, the ε for 5A-HBO is higher than that of its parent molecule HBO (ε_{DCM} (333 nm) = 0.34 x 10^3 M^{-1} cm^{-1}),[41] showing the positive effect of the amino substituent in the oscillator strength of the related transition.

The fluorescence emission spectra of 5A-MBO consist of a unique band whose maximum is shifted with the solvent nature: 400, 450, 475 and 490 nm in n-heptane, DCM, THF and ACN, respectively (Figure 3). The large Stokes-shift of the emission spectra (5200, 7900, 8200 and 9350 cm^{-1} for n-heptane, DCM, THF and ACN, respectively) reflects an intramolecular charge transfer (ICT) taking place in the excited state from the amino group to the MBO part, as it has been previously reported for other molecules.[24, 32, 33] The emission spectra of 5A-HBO exhibit different behaviour. While in n-heptane the emission spectrum displays a dual emission with maxima located at 400 and 500 nm, those of DCM, THF and ACN solution are not very different from the obtained for 5A-MBO. The two emission bands observed for 5A-HBO in n-heptane solution are assigned to the open-enol charge-transfer (open-ECT) (400 nm) and keto (K) (500 nm) species (Scheme 1). The large stokes shift (4500 cm^{-1}) observed for the enol emission band (comparable to that observed for 5A-MBO) indicates an ICT reaction in the excited state of this specie leading to a charge redistribution within the molecular frame increasing the dipole moment, as we have previously demonstrated for comparative derivative (6A-HBO).[24, 32] This is in agreement with the theoretical results where a high value in the dipole moment is observed for the relaxed excited enol specie (E*) (~ 4 D). The emission of 5A-HBO in DCM solution displays a broader band when compared to the 5A-MBO, which suggest the presence of at least two emitters in this region. Time-resolved experiments (see below) will shine more light in this behaviour. Some hydroxyflavones derivatives, like 4'-dimethylaminoflavonol (DMAF), show a similar behaviour in this solvent.[27, 30] Finally, 5A-HBO in ACN and THF solutions exhibit a unique band very similar to that observed for 5A-MBO indicating that the emission is due to open-enol charge-transferred forms (open-ECT). Here, the solvent molecules are interacting with the dye inhibiting the intramolecular proton motion

(Scheme 1). The same behaviour in a stronger H-bond acceptor solvent (N, N-dimethylformamide, DMF) was observed for this molecule.[33] The fluorescence excitation spectra of 5A-MBO and 5A-HBO in the related solvents exhibit the same behaviour than that observed for the absorption one, indicating that the emitters are coming from a common origin in the ground state (Figure S1 and S2 in ESI†).

The presence of the amino group in the HBO structure increases the electronic density of the molecule, producing changes in its spectral behaviour.[24, 32, 33] The theoretical results show the differences between HBO and 5A-HBO. At S_0, HBO has the electronic density mostly localized in the phenol part, while for 5A-HBO it is in the benzoxazole one. However, at S_1 and using the result of a vertical excitation (without change in geometry) the electronic density is redistributed for all molecular structure (Figure 1). In HBO, the electronic density migrates from the phenol part to the benzoxazole one, while in 5A-HBO we got the reverse trend. The pKa and pKa* values, which were reported in previous studies,[1, 33, 42] also reflect the differences between HBO and 5A-HBO (Table S2 in ESI†). At S_0, pKa's of the imino group ($-NH^+=$) for HBO and 5A-HBO are -0.3 and 4.2, respectively, while those of the -OH group are 10.40 and 10.15. Thus and according to the theoretical results, for 5A-HBO due to the increase of the electronic density by the presence of the amino group, the pKa of ($-NH^+=$) is higher. On the other hand, at S_1, pKa's of the ($-NH^+=$) for HBO and 5A-HBO are 5.24 and 7.76 while pKa's of the -OH group are -0.04-1.35, and 5.02, respectively. Now, the higher pKa*(OH) value for 5A-HBO, shows a decrease in the acidity of this group when compared to HBO. Moreover, a high difference of the acidity/basicity at S_1 between the donor and acceptor groups is necessary to produce the ESIPT reaction. This difference, ΔpKa* (pKa* (-N=) – pKa* (OH-)) is ~5 for HBO while it is only 2.74 for 5A-HBO. The small difference observed for 5A-HBO reflects the slowing down on the ESIPT reaction rate in apolar or less polar solvents (n-heptane and DCM) and its absence in H-bond acceptor solvents (ACN and THF).

3.3 Picosecond Time-Resolved Fluorescence Study

To shed light on the different behaviours observed above, the ps-emission decays of 5A-MBO and 5A-HBO in the same solutions were recorded upon excitation at 371 nm. To begin with the 5A-MBO behaviour, Figure 4A shows representative

results observing at 475 nm. The decays were well fitted using a monoexponential function giving time constants of 2.5, 5.0, 6.8 and 7.2 ns for n-heptane, DCM, THF and ACN, respectively. The lifetimes correspond to the emission of the excited ICT species.

The photodynamical behaviour of 5A-HBO depends on the solvent (Figure 4B and 2C). To make easy the discussion of obtained results, we begin with the n-heptane solution where a multiexponential behaviour is observed (Figure 4B). Table 2 gives the obtained time constants (τ_i), amplitudes (A_i), pre-exponential factors (a_i) and relative contributions (c_i) normalized to 100. The 20-ps component is decaying at the bluest part (400-450 nm), while it is rising at the reddest one (475-550 nm). The 810-ps component (appearing from 410 nm) is decaying at all observation wavelengths, and increasing its contribution at the reddest part of the spectrum. The 2.5-ns component is present up to 450 nm being its contribution longer at the bluest part. Based on these results, the 2.5-ns component, similar to that obtained for 5A-MBO, is assigned to an open-ECT form, while the 810-ps one is due to the keto type tautomer (K). The 20-ps component which is decaying in the enol (E) emission region and rising in the K one, corresponds to the ESIPT reaction which takes place in the excited E form to produce the K tautomer (Scheme 2A). Note that for HBO in apolar solvents, the ESIPT reaction occurs in <150 fs,[31] shorter than the observed for 5A-HBO in the same solvent. The theoretical studies at S_1 in gas phase show that the energy differences between the relaxed excited enol form (E*) and transition state (TS*) are lower for HBO (1.39 kcal/mol) than for 5A-HBO (3.94 kcal/mol). Moreover, for HBO at S_1, the keto energy compared to that of E* is stabilized by ~3 kcal/mol, while for 5A-HBO this difference is only 0.32 kcal/mol. Therefore, the slow ESIPT reaction for 5A-HBO is in agreement with the theoretical results showing a higher energy barrier on the TS*, and a less stabilization on its keto form. Similar observations were described for another proton coupled charge transfer dyes.[23, 27, 32]

Figure 4C displays representative emission decays of 5A-HBO in DCM solution, while Table 3 gives the obtained values τ_i, A_i, a_i and c_i. The decays exhibit a biexponential behaviour giving time constants of τ_1= 2 ns, which is decaying at all observation wavelengths, and τ_2= 500 ps, decaying at the bluest part (for wavelengths shorter than 475 nm) and rising at the reddest one (for wavelengths longer than 475 nm). The ratio of the amplitudes at the reddest part of the spectra (650 nm) is $A_2/A_1 \approx -1$ (Table 3), which is an essential condition for a kinetic scheme modeling reversible reaction in the excited state.[24, 27] To shed more light on the reversibility of ESIPT

reaction of 5A-HBO in DCM, time-resolved emission spectra (TRES) were recorded. In this spectrum the shape of the broad emission band, where we have two emitters, does not change after of ~1 ns suggesting that both excited species are equilibrated (Figure 5). Therefore, 500-ps and 2-ns components reflect the combination of forward (or direct) and back (or reverse) proton motion, and the ECT and K emission lifetimes, respectively. To analyze the reversibility of this reaction, the direct (k_{DPT}) and reverse (k_{RPT}) proton motion rate constants together with the keto lifetime ($\tau(K)$) were calculated through equations S1-S6 (ESI†), in which we suppose that the ECT lifetime has a similar value to that observed for 5A-MBO (5 ns), where the proton motion does not occur (Scheme 2B). The obtained values are $\tau(K)$ = 950 ps, $k_{DPT} = 6.4 \times 10^8$ s^{-1} and $k_{RPT} = 6.1 \times 10^8$ s^{-1}. The k_{DPT} and k_{RPT} constants are very similar, showing that the ESIPT reaction is extremely equilibrated ($K = k_{DPT}/ k_{RPT} = 1.05$). This is in agreement with the relative intensities (close to one) of the dual emission observed in the broad emission spectrum (Figure 3). To further explore the behaviour of the reversible ESIPT reaction, a kinetic isotopic (OH/OD) effect study using the deuterated molecule (5A-DBO) in DCM-d_2 was realized. We do not observed change in the emission signal indicating the absence of tunneling (Figure S3 in ESI†). Thus, the direct and reverse ESIPT reactions have to overcome the barrier along the IHB and solvent coordinates.[24]

Finally, the emission decays of 5A-HBO in THF and ACN solutions were recorded and fitted using a monoexponential function giving time constants of 6.2 and 6.8 ns, respectively. These time constants, larger than those observed in n-heptane (1.65 ns) and DCM (5.0 ns), are very similar to those obtained for 5A-MBO in the same solvents (6.8 and 7.2 ns, respectively). Thus, we believe that the intramolecular proton motion for 5A-HBO in THF and ACN solutions does not occur. Therefore, the emission observed for 5A-HBO is due to open-ECT species, produced by the breaking of the IHB owing to the interactions with solvent molecules, having a H-bond acceptor ability (β= 0.55 (THF) and 0.4 (ACN)) (Scheme 2C). This behaviour was also observed in a more basic solvent (DMF) where the open-ECT emission lifetime was 7.3 ns.[33]

To get information on the radiationless decays, we measured fluorescence quantum yields (φ). In n-heptane and DCM, where the ESIPT reaction takes place, the global φ of 5A-HBO (0.09 and 0.2, respectively) are smaller than those obtained for its methylated compound (0.26 and 0.38, respectively) (Table 3). The non-radiative constants (k_{nr}) for 5A-HBO in DCM solution (reversible ESIPT reaction) were calculated through eqs S7 and S8 (ESI†) and using the experimental quantum yields (φ)

for each species (Table 3). k_{nr} values show that K species undergo more efficient non-radiative processes than ECT ones (k_{nr} (ECT) = $4.0x10^8$ s^{-1} and k_{nr} (K) = $1.1x10^9$ $s^{-1}$for n-heptane, and k_{nr} (ECT) = $1.7x10^8$ s^{-1} and k_{nr} (K) = $9.9x10^8$ $s^{-1}$for DCM). However, in THF and ACN solutions, where the ESIPT reaction does not occur, the φ values for 5A-HBO (0.39 and 0.36, for THF and ACN, respectively) are similar to those obtained for 5A-MBO in the same solvents (0.39 and 0.37, respectively).

3.4 Femtosecond dynamics

The ultrafast dynamics of 5A-MBO and 5A-HBO in the same solutions were studied. Exciting at 360 nm, the molecular system is brought to almost without excess of vibrational energy at S_1. Figure 6 shows the fluorescence transients of 5A-MBO in the related solvents. Tables 3 and 4 give the results for 5A-MBO and 5A-HBO of the multiexponential fits, taking into account the ps-results discussed above.

To begin with, the ultrafast behaviours of 5A-MBO were investigated. The longest components (in the range of nanoseconds) are fixed in the fit taking into account the results obtained from the TCSPC measurements (see the preceding section). 5A-MBO exhibits a comparable behaviour in all used solvents, showing two components, an ultrafast one of 200-300 fs (except for n-heptane), present only at the bluest part as a decay, and another of 0.7-1.2 ps, which is decaying at bluest part and rising (except for n-heptane) at the reddest one. The ultrafast component is assigned to intramolecular vibrational energy redistribution (IVR), value comparable to the obtained for molecules of similar size.[43-45] As we explained above (steady-state part) due to the red-shift observed in the emission spectra, an ultrafast ICT is expected. However, the ultrafast ICT is not observed here, on the contrary to our previous study where an ultrafast rise component (80-140 fs) was recorded for a similar derivative (6A-MBO).[24, 32] Thus, we suggest the ICT process takes place in less than ~50 fs (resolution of the system after deconvolution). The lack of the ultrafast component observation owing to ICT and IVR processes in n-heptane could be a compensation of these rise (ICT) and decay (IVR) components at the bluest part (Table 4). On the other hand, the 0.7-1.2 ps component, which is decaying at the bluest part and rising (except for n-heptane) at the reddest one, is assigned to solvent relaxation processes. Note that solvent relaxation times for DCM (1 ps) and ACN (0.6 ps) studied in coumarin 153 (C153) are similar to those obtained here for the same solvents (1.2 and 0.7 ps for DCM and ACN, respectively).[46]

Finally, the ultrafast dynamics of 5A-HBO in the same solvents were examined. 5A-HBO (Figure 7) shows an ultrafast behaviour similar to that of the observed one of 5A-MBO (Table 5) exhibiting an ultrafast component of 200-300 fs and another longer one of 0.7-1.2 ps, assigned to the same processes as in the methylated derivative. This is in agreement with what we observed in the emission spectra: for THF and ACN solutions both molecules behave equal, and for n-heptane and DCM solutions, we observe the ECT emission band for both molecules at the same region. Thus, we believe

that for 5A-HBO (like in 5A-MBO) an ICT process of <50 fs takes place. The occurrence of this event is supported by theoretical results where we observed charge redistribution together with an increase in the dipole moment of the excited and relaxed enol specie. Moreover, 5A-HBO in n-heptane shows an additional component of 20 ps, which is similar to that observed in the picosecond experiment, assigned to the ESIPT process (Figure S5A in ESI†). It remarkable that the ultrafast ICT reaction (<50 fs), triggered by the amino group, slows down the ESIPT one in n-heptane, while in DCM solution it makes reversible; and in THF and ACN solutions, it does not occur (Scheme 2). In these two media, a breaking of the IHB produced by the specific interactions with the solvent molecules occur, producing solvated open-enol forms with emission spectrum and dynamics similar to those of the 5A-MBO. To summarize, Schemes 2A, B and C give the possible mechanisms of the three different behaviours taking place at S_1 of 5A-HBO in n-heptane, DCM, ACN and THF solutions.

As we explained above, the $–NH_2$ presence increases the electronic density at the S_0 and S_1 states, producing changes in the absorption, emission and photodynamical behaviour of 5A-HBO. For example, when we compare 5A-HBO with HBO in apolar solvent (n-heptane), the ESIPT reaction of the former is slower (20 ps vs 150 fs)[31] and has to overcome a higher energy barrier, as suggested by the TD-DFT theoretical results. The $–NH_2$ position also affects the ESIPT reaction rate constant. For 6A-HBO in n-heptane, the reaction is faster (1 ps) than the 5A-HBO one (20 ps).[32] On the other hand, 6A-HBO in ACN and THF solutions, presents a reversible behaviour where the ESIPT reaction takes place in a hundred of picoseconds.[24] However, 5A-HBO in these solvents does not present any proton motion exhibiting only a breaking of the IHB. The amino group in –para (6A-HBO) or –meta (5A-HBO) position affects the electronic densities on the –N= and OH- sites, leading to a change in their acidities (Table S2 in ESI†) at both ground and excited states. We have therefore demonstrated that the presence and position of the amino group in the benzoxazole part modulate the behaviour and rate of the ESIPT reaction.[24, 32]

4. Conclusion

In this work, we reported on spectroscopic and photodynamical behaviours of 5A-HBO in n-heptane, DCM, THF and ACN solutions. We also performed theoretical calculations (TD-DFT), in gas phase, for which the results for HBO (molecule without amino group) and 5A-HBO show that presence of the $–NH_2$ group in the molecular framework induces an increase of the electronic density in the benzoxazole part. Moreover, the relaxed excited enol specie (E*) of 5A-HBO presents a dipole moment (~4 D) higher than that of HBO (0.3 D). These results indicate that for excited 5A-HBO an ICT process occurs followed by an ESIPT reaction.

Steady-state emission studies of 5A-HBO and 5A-MBO shows that the former in n-heptane and DCM solutions undergoes and ICT event followed by a proton transfer motion. While in ACN and THF solutions, we only observed the ICT emission band. Femtosecond studies for 5A-HBO in all used solvents, suggest an ultrafast ICT reaction (<50 ps) and a solvent relaxation (0.7-1.2 ps). These results are comparable and discussed to those of the methylated derivative (5A-MBO) which does not suffer any ESIPT reaction. Following the ICT reaction, 5A-HBO in n-heptane solution shows an irreversible and remarkably slow (20 ps) ESIPT one. These results are in agreement with those of the DFT ones in gas phase, showing an almost similar energy of both ECT* and K* forms, between which the transitions-state energy is ~ 4 kcal/mol. Both experimental and theoretical result of 5A-HBO and HBO are in agreement and show the effect of the amino group in the coupled ICT and ESIPT reactions. In DCM solution, a subsequent and reversible proton transfer reactions takes place in the ns-regime. The isotopic effect in this solvent is not observed indicating that the direct and reverse reactions have to overcome energy barriers using the IHB and solvent coordinates. Finally, in THF and ACN solutions the ESIPT reaction does not occur owing to the breaking of the IHB originated by intermolecular interactions between solvent and 5A-HBO molecules. Our results shed more light on the substituent effect on the ICT and ESIPT reactions, opening the way to more exploration of these coupled reactions, which might be need for better design of materials based on charge and proton transfer events.

Acknowledgments

This work was supported by the MINECO through projects: Consolider Ingenio 2010 (CSD2009-0050, MULTICAT), and MAT2011-25472. M.G. thanks the MINECO for the Ph.D. fellowship.

Electronic Supplementary Information (ESI†) available: Figure S1 and S2 show the excitation fluorescence and absorption spectra of 5A-MBO and 5A-HBO in different solvent, respectively. Figure S3 presents magic-angle emission decays of 5A-HBO and 5A-DBO in DCM and DCM-d_2 solutions, respectively. Table S1 contains the Cartesian coordinates of the calculated geometries. Table S2 shows the pKa's values for HBO, 6A-HBO and 5A-HBO at S_0 and S_1.

References

1. M. Krishnamurthy and S. K. Dogra, *J. Photochem.*, 1986, **32**, 235-242.
2. A. Costela, J. M. Muñoz, A. Douhal, J. M. Figuera and A. U. Acuña, *Appl. Phys. B*, 1989, **49**, 545-552.
3. A. Douhal, S. K. Kim and A. H. Zewail, *Nature*, 1995, **378**, 260-263.
4. A. Douhal, F. Lahmani and A. H. Zewail, *Chem. Phys.*, 1996, **207**, 477-498.
5. T. Elsaesser and H. J. e. Bakker, eds., *Ultrafast Hydrogen Bonding Dynamics and Proton Transfer Processes in the Condensed Phase*, Kluwer Academic Publisher, 2002.
6. M. Rini, J. Dreyer, E. T. J. Nibbering and T. Elsaesser, *Chem. Phys. Lett.*, 2003, **374**, 13-19.
7. G. Zhang, H. Wang, Y. Yu, F. Xiong, G. Tang and W. Chen, *Appl. Phys. B*, 2003, **76**, 677-681.
8. M. Ziolek, J. Kubicki, A. Maciejewski, R. Naskrecki and A. Grabowska, *Phys. Chem. Chem. Phys.*, 2004, **6**, 4682-4689.
9. E. T. J. Nibbering, H. Fidder and E. Pines, *Annu. Rev. Phys. Chem.*, 2005, **56**, 337-367.
10. S.-J. Lim, J. Seo and S. Y. Park, *J. Am. Chem. Soc.*, 2006, **128**, 14542-14547.
11. J. T. K. Hynes, J. P.; Limbach, H. -H.; Limbach, R. L. (eds), ed., *Hydrogen-Transfer Reactions*, 1 st vol: I-IV edn., Wiley-VCH Weinheim, Germany, 2007.
12. O. F. Mohammed, S. Luber, V. S. Batista and E. T. J. Nibbering, *J. Phys. Chem. A*, 2011, **115**, 7550-7558.
13. J. E. Kwon and S. Y. Park, *Adv. Mater.*, 2011, **23**, 3615-3642.
14. J. Zhao, S. Ji, Y. Chen, H. Guo and P. Yang, *Phys. Chem. Chem. Phys.*, 2012, **14**, 8803-8817.
15. P. Wnuk, G. Burdzinski, M. Sliwa, M. Kijak, A. Grabowska, J. Sepiol and J. Kubicki, *Phys. Chem. Chem. Phys.*, 2014, **16**, 2542-2552.
16. S. Kim, J. Seo, H. K. Jung, J. J. Kim and S. Y. Park, *Adv. Mater.*, 2005, **17**, 2077-2082.
17. W. Sun, S. Li, R. Hu, Y. Qian, S. Wang and G. Yang, *J. Phys. Chem. A*, 2009, **113**, 5888-5895.
18. A. Douhal, F. Amat-Guerri, M. P. Lillo and A. U. Acuna, *J. Photochem. and Photobiol. A: Chemistry*, 1994, **78**, 127-138.
19. O. K. Abou-Zied, R. Jimenez, E. H. Z. Thompson, D. P. Millar and F. E. Romesberg, *J. Phys. Chem. A*, 2002, **106**, 3665-3672.

20. D. P. Zhong, A. Douhal and A. H. Zewail, *Proc. Natl. Acad. Sci. U.S.A.*, 2000, **97**, 14056-14061.
21. Y.-M. Cheng, S.-C. Pu, C.-J. Hsu, C.-H. Lai and P.-T. Chou, *ChemPhysChem*, 2006, **7**, 1372-1381.
22. Y.-M. Cheng, S.-C. Pu, Y.-C. Yu, P.-T. Chou, Huang, C.-T. Chen, T.-H. Li and W.-P. Hu, *J. Phys. Chem. A*, 2005, **109**, 11696-11706.
23. A. Douhal, M. Sanz, M. A. Carranza, J. A. Organero and L. Santos, *Chem. Phys. Lett.*, 2004, **394**, 54-60.
24. M. Gutierrez, N. Alarcos, M. Liras, F. Sánchez and A. Douhal, *J. Phys. Chem. B*, 2015, **119**, 552-562.
25. S. Hammes-Schiffer and A. A. Stuchebrukhov, *Chem. Rev.*, 2010, **110**, 6939-6960.
26. C.-C. Hsieh, Y.-M. Cheng, C.-J. Hsu, K.-Y. Chen and P.-T. Chou, *J. Phys. Chem. A*, 2008, **112**, 8323-8332.
27. A. D. Roshal, J. A. Organero and A. Douhal, *Chem. Phys. Lett.*, 2003, **379**, 53-59.
28. J. Seo, S. Kim and S. Y. Park, *J. Am. Chem. Soc.*, 2004, **126**, 11154-11155.
29. C. H. Kim, J. Park, J. Seo, S. Y. Park and T. Joo, *J. Phys. Chem. A*, 2010, **114**, 5618-5629.
30. V. V. Shynkar, Y. Mély, G. Duportail, E. Piémont, A. S. Klymchenko and A. P. Demchenko, *J. Phys. Chem. A*, 2003, **107**, 9522-9529.
31. H. Wang, H. Zhang, O. K. Abou-Zied, C. Yu, F. E. Romesberg and M. Glasbeek, *Chem. Phys. Lett.*, 2003, **367**, 599-608.
32. N. Alarcos, M. Gutiérrez, M. Liras, F. Sánchez and A. Douhal, *Phys. Chem. Chem. Phys. DOI: 10.1039/C5CP00577A*, 2015.
33. N. Alarcos, M. Gutiérrez, M. Liras, F. Sánchez and A. Douhal, *Photochem. Photobiol. Sci.*, 2015, **Submitted**.
34. T. Yanai, D. P. Tew and N. C. Handy, *Chem. Phys. Lett.*, 2004, **393**, 51-57.
35. P. C. Hariharan and J. A. Pople, *Theor. Chim. Acta*, 1973, **28**, 213-222.
36. M. M. Francl, W. J. Pietro, W. J. Hehre, J. S. Binkley, M. S. Gordon, D. J. DeFrees and J. A. Pople, *J. Chem.Phys.*, 1982, **77**, 3654-3665.
37. M. J. Frisch, G. W. Trucks, H. B. Schlegel, G. E. Scuseria, M. A. Rob, J. R. Cheeseman, G. Scalmani, V. Barone, B. Mennucci, J. Montgomery, K. N. T. Vreven, J. C. Kudin, J. M. Burant, S. S. Millam, J. Iyengar, V. Tomasi, G. Cossi, G. A. Rega and H. N. Petersson, M. Hada, M. Ehara, K. Toyota, R. Fukuda, J. Hasegawa, M. Ishida, T. Nakajima, Y. Honda, O. Kitao, H. Nakai, M. Klene, X. Li, J. E. Knox, H. P. Hratchian, J. B. Cross, V. Bakken, C. Adamo, J. Jaramillo, R. Gomperts, R. E. Stratmann, O. Yazyev, A. J. Austin, R. Cammi, C. Pomelli, J. W. Ochterski, P. Y. Ayala, K. Morokuma, G. A. Voth, P. Salvador, J. J. Dannenberg, V. G. Zakrzewski, S. Dapprich, A. D. Daniels, M. C. Strain, O. Farkas, D. K. Malick, A. D. Rabuck, K. Raghavachari, J. B. Foresman, J. V. Ortiz, Q. Cui, A. G. Baboul, S. Clifford, J. Cioslowski, B. B. Stefanov, G. Liu, A. Liashenko, P. Piskorz, I. Komaromi, R. L. Martin, D. J. Fox, T. Keith, M. A. Al-Laham, C. Y. Peng, A. Nanayakkara, M. Challacombe, P. M. W. Gill, B. Johnson, W. Chen, M. W. Wong, C. Gonzalez, and J. A. Pople, Gaussian Inc., Wallingford CT, 2004.
38. R. A. Velapoldi and K. D. Mielenz, *Appl. Opt.*, 1981, **20**, 1718-1718.
39. J. A. Organero, L. Tormo and A. Douhal, *Chem. Phys. Lett.*, 2002, **363**, 409-414.
40. M. Gil and A. Douhal, *Chem. Phys. Lett.*, 2006, **428**, 174-177.
41. A. Mordzinski and K. H. Grellmann, *J. Phys. Chem.*, 1986, **90**, 5503-5506.
42. E. L. Roberts, J. Dey and I. M. Warner, *J. Phys. Chem.*, 1996, **100**, 19681-19686.
43. T. Elsaesser and W. Kaiser, *Chem. Phys. Lett.*, 1986, **128**, 231-237.
44. N. P. Ernsting, S. A. Kovalenko, T. Senyushkina, J. Saam and V. Farztdinov, *J. Phys. Chem. A*, 2001, **105**, 3443-3453.
45. N. Alarcos, B. Cohen and A. Douhal, *J. Phys. Chem. C*, 2014, **118**, 19431-19443.
46. M. L. Horng, J. A. Gardecki, A. Papazyan and M. Maroncelli, *J. Phys. Chem.*, 1995, **99**, 17311-17337.

Caption of figures, schemes and tables.

Scheme 1. Possible molecular structures of 5A-MBO and 5A-HBO.

Scheme 2. Suggested photodynamics mechanisms of 5A-HBO in A) n-heptane, B) DCM, and C) ACN and THF solutions, involving ICT and ESIPT reactions and IHB breaking. The arrows indicate the nature of the photoreaction in the related structure and the values gives dynamical and photophysical parameters..

Table 1. A) Total Mulliken charges (in au) of the phenol part for HBO and 5A-HBO in gas phase at different states. B) Dipole moment variations ($\Delta\mu$ in Debye) for HBO and 5A-HBO due to the indicated photochemical processes.

Table 2. Values of the time constants (τ_i), normalized (to 100) pre-exponential factors (a_i) and fractional contributions ($c_i = \tau_i a_i$) obtained from a multiexponential fit of the ps-ns emission decays of 5A-HBO in n-heptane and DCM solutions, upon excitation at 371 nm, and at the observation wavelengths as indicated. The negative sign for a_i (c_i) indicates a rising component in the emission signal.

Table 3. Values of the photophysical parameters of 5A-HBO in a DCM solution. τ and φ are fluorescence lifetime and quantum yield, respectively. k_r and k_{nr} are the radiative and nonradiative rate constants, respectively.

Table 4. Values of the time constants (τ_i), normalized (to 100) pre-exponential factors (a_i) of the function used in fitting the femtosecond emission transient of 5A-MBO in different solutions, upon excitation at 360 nm, and observation as indicated. The negative sign for a_i (c_i) indicates a rising component in the emission signal.

Table 5. Values of the time constants (τ_i), normalized (to 100) pre-exponential factors (a_i) of the function used in fitting the femtosecond emission transient of 5A-HBO in different solutions, upon excitation at 360 nm, and observation as indicated. The negative sign for a_i (c_i) indicates a rising component in the emission signal.

Figure 1. Shape of the HBO and 5A-HBO HOMO/LUMO orbitals involved in the electronic excitation from the ground to the lowest singlet excited electronic state.

Figure 2. Energy profiles in the ground (S_0) and first singlet excited (S_1) electronic states for HBO and 5A-HBO in gas phase. The obtained energies of E*(FC), relaxed E*, transition state (TS*), K* and ground state, E and K forms are given in kcal/mol. For clarity, the scheme is not in scale.

Figure 3. Normalized UV-visible absorption and fluorescence spectra (upon excitation at 350 nm) of 5-MBO (dashed lines) and 5A-HBO (solid lines) in the solvents indicated in the inset.

Figure 4. Magic-angle emission decays of (A) 5A-MBO in (1) n-heptane, (2) DCM, (3) THF and (4) ACN solutions and of 5A-HBO in (B) n-heptane and (C) DCM solutions. The excitation wavelength was 371 nm and the observation as indicate in the inset. The solid lines are from the best fit using multiexponential functions, and the IRF is the instrumental response function. To visualize the single exponential behavior of the decays in panel (A) we plotted the signal in a logarithmic scale.

Figure 5. Normalized (to the maximum of the intensity) time-resolved emission spectra (TRES) of 5A-HBO in a DCM solution upon excitation at 371 nm and gated at indicated at different times after the pulse excitation.

Figure 6. Femtosecond emission transients of 5A-MBO in (A) n-heptane, (B) DCM, (C) THF and (D) ACN solutions. The samples were excited at 360 nm and recorded at the indicated wavelengths. The solid lines are from the best multiexponential fit and the IRF is the instrumental response function (220 fs).

Figure 7. Magic-angle fs-emission transients of 5A-HBO in (A) n-heptane, (B) DCM, (C) THF and (D) ACN solutions. The samples were excited at 360 nm and monitored at the indicated wavelengths. The solid lines are from the best multiexponential fits. IRF is the instrumental response function (220 fs).

Scheme 1.

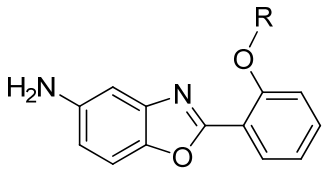

open-enol

$R=CH_3$ 5A-MBO
R=H 5A-HBO

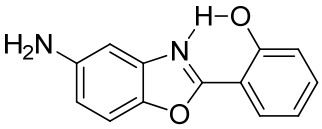

syn-enol

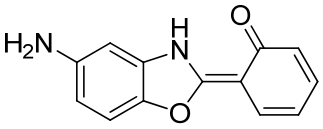

keto

Scheme 2.

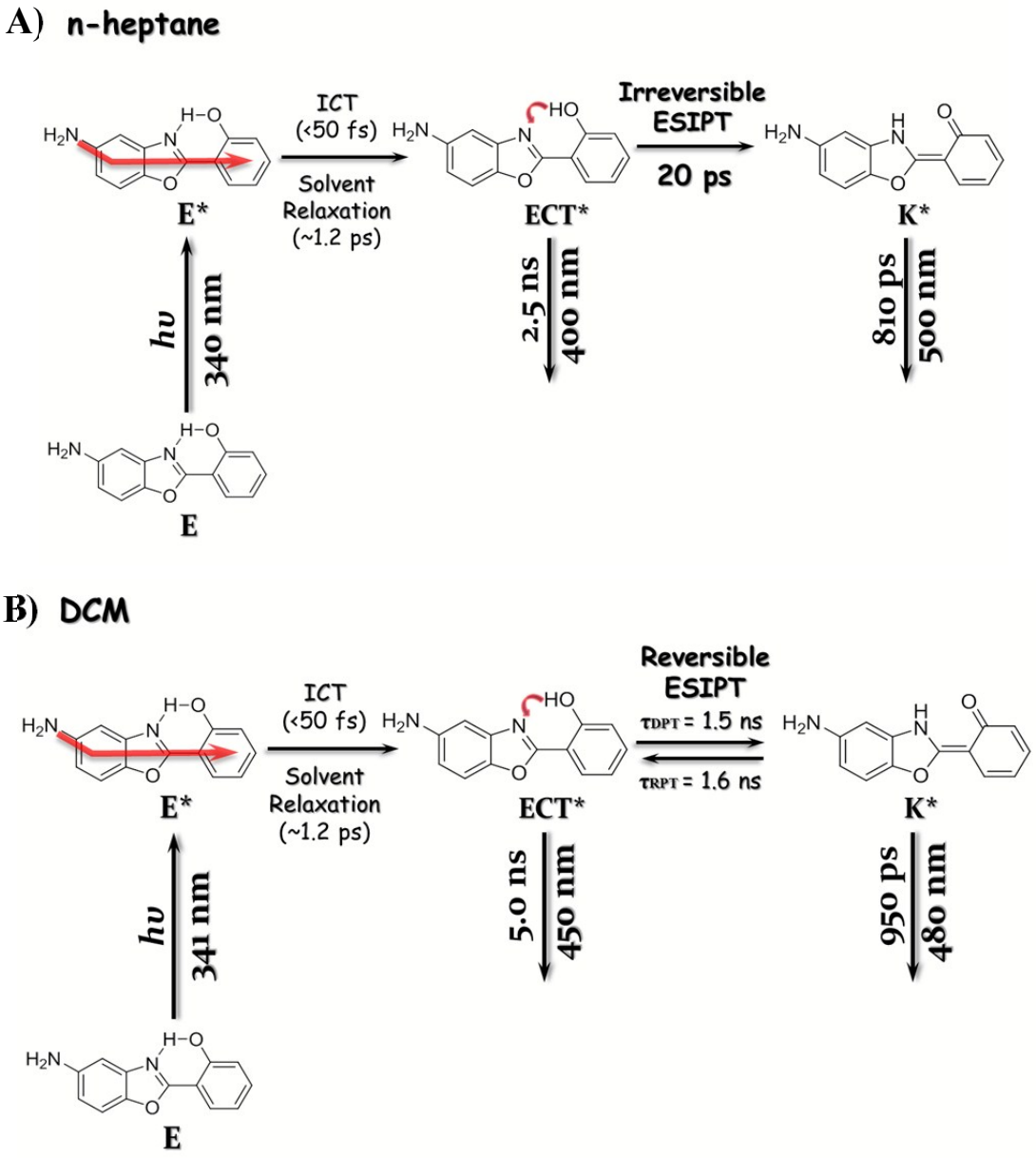

C) ACN

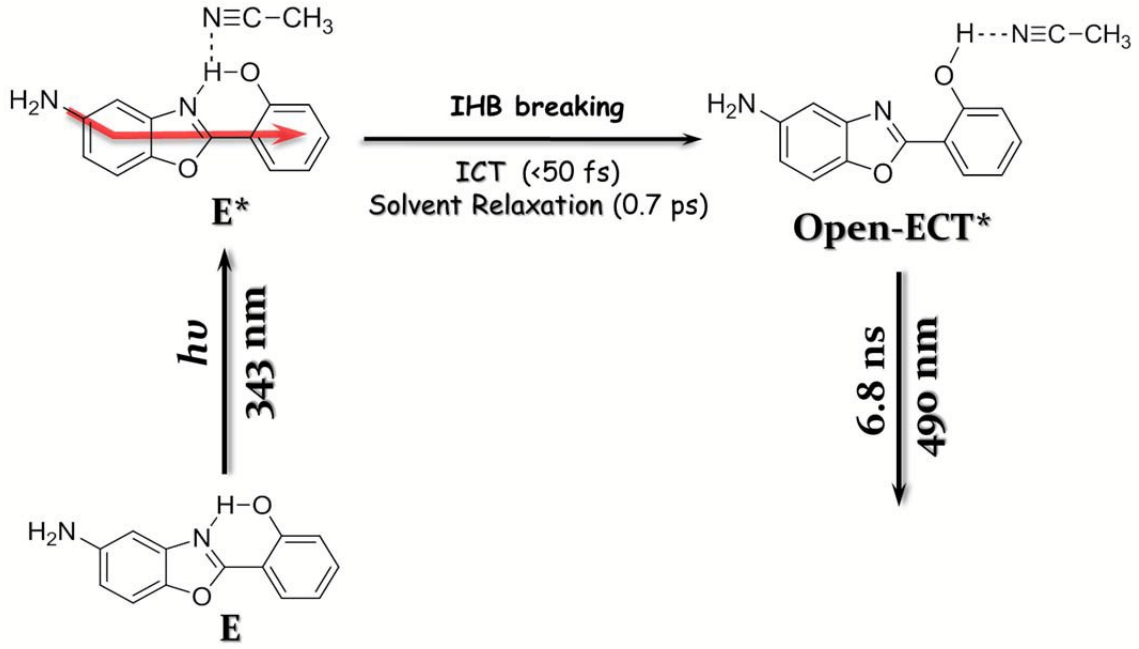

D) THF

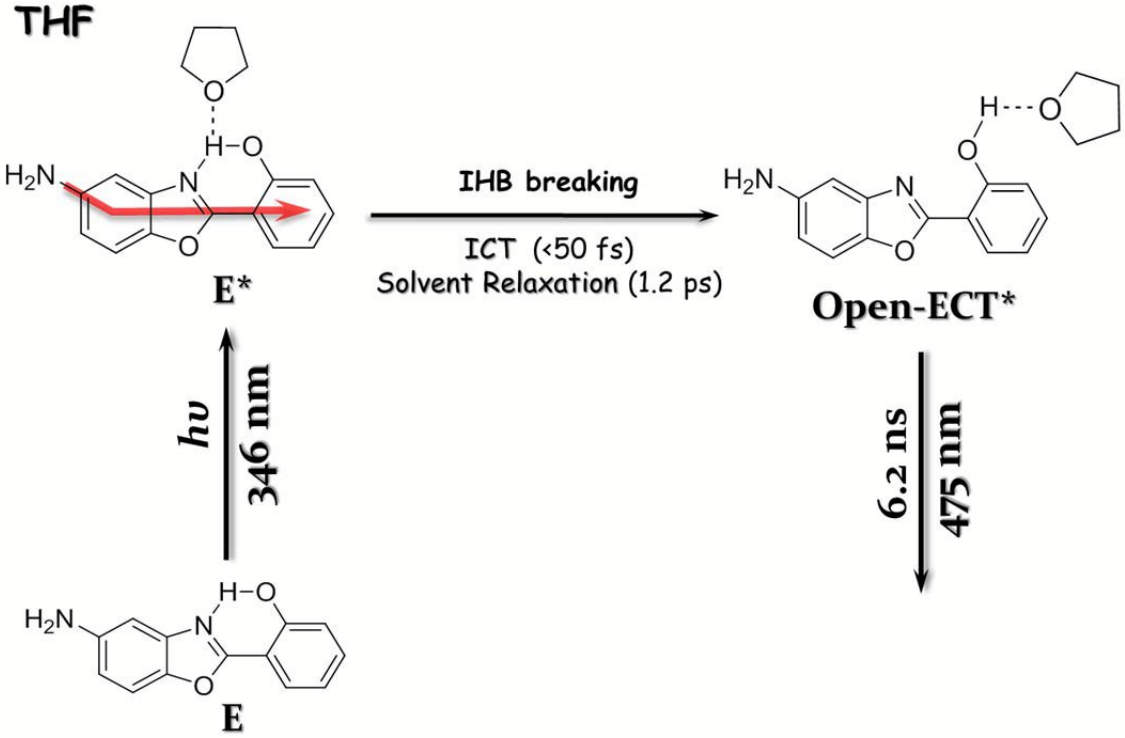

Figure 1.

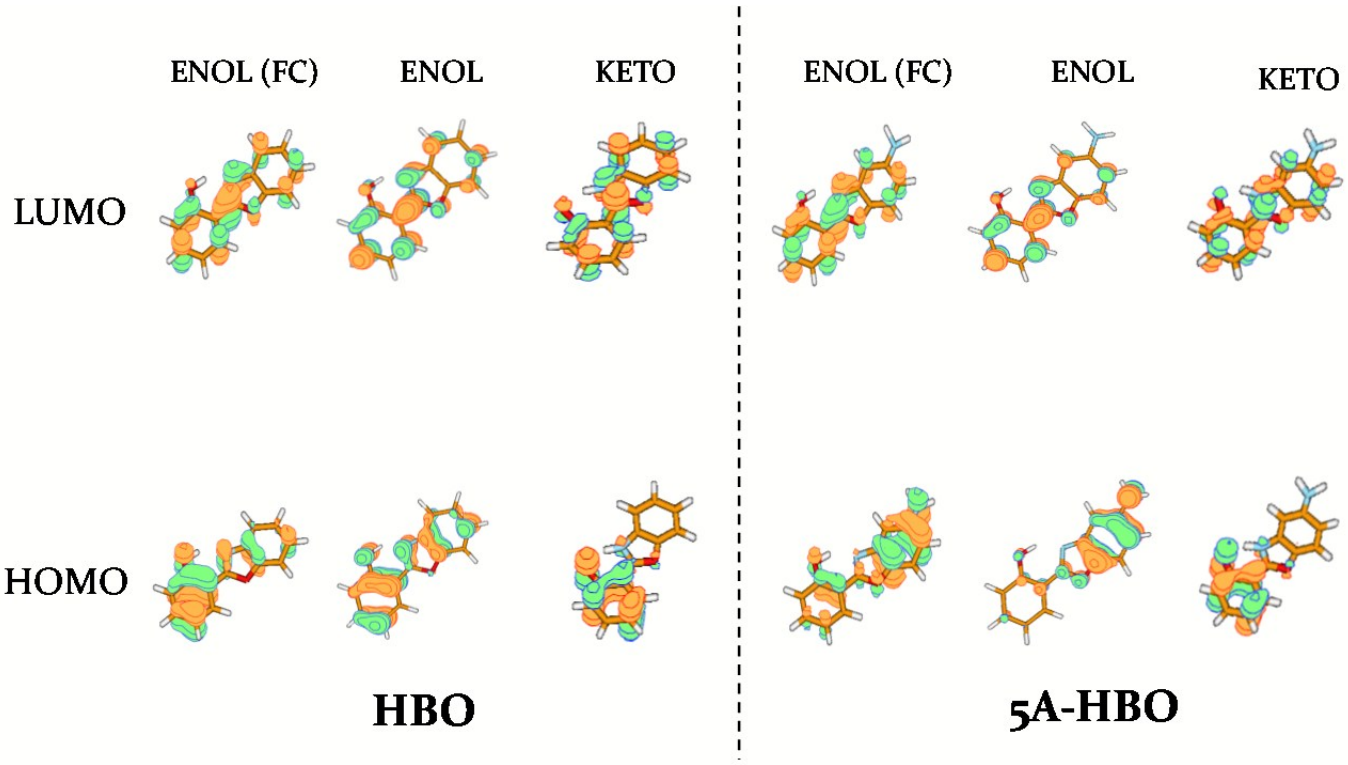

Figure 2.

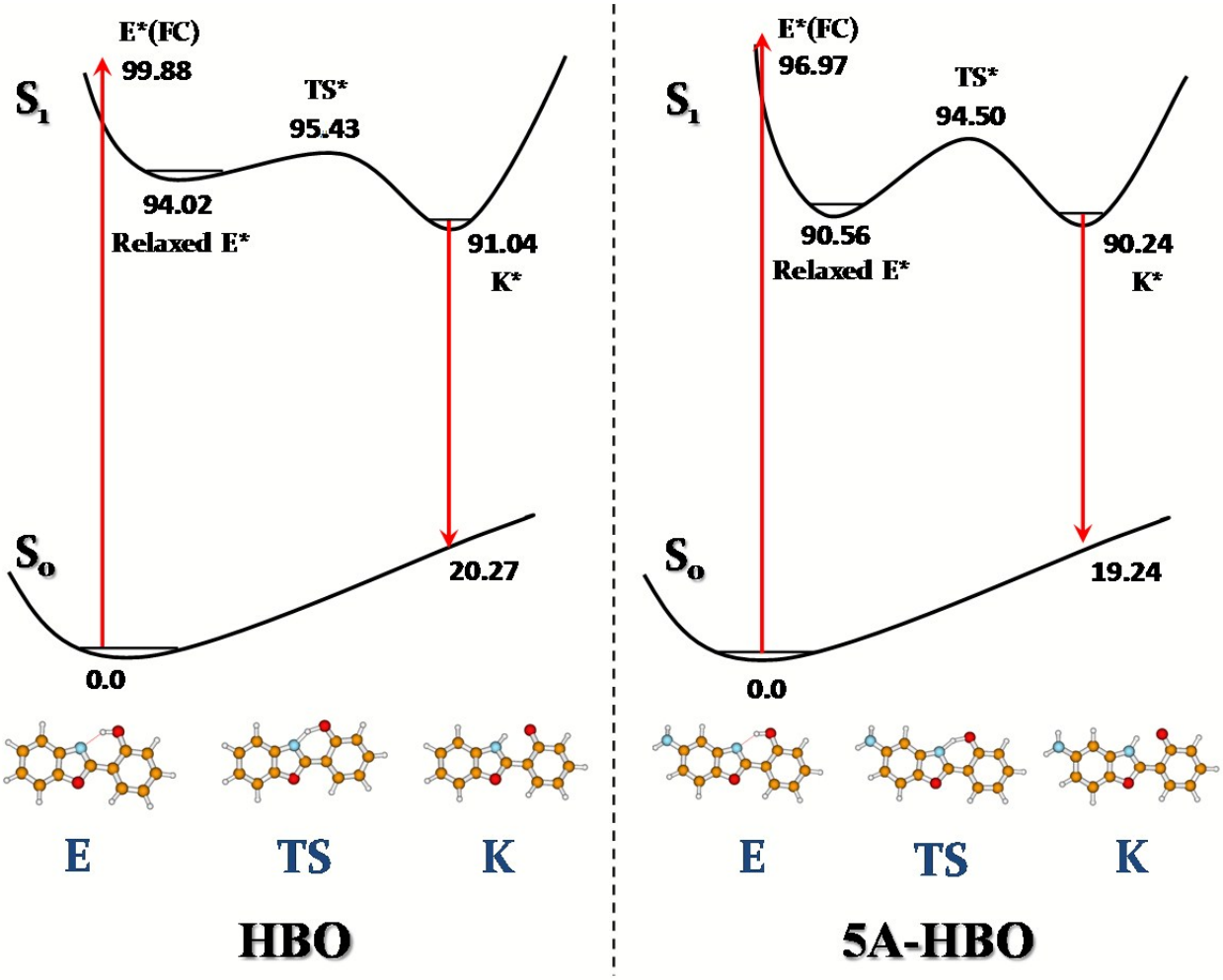

Figure 3.

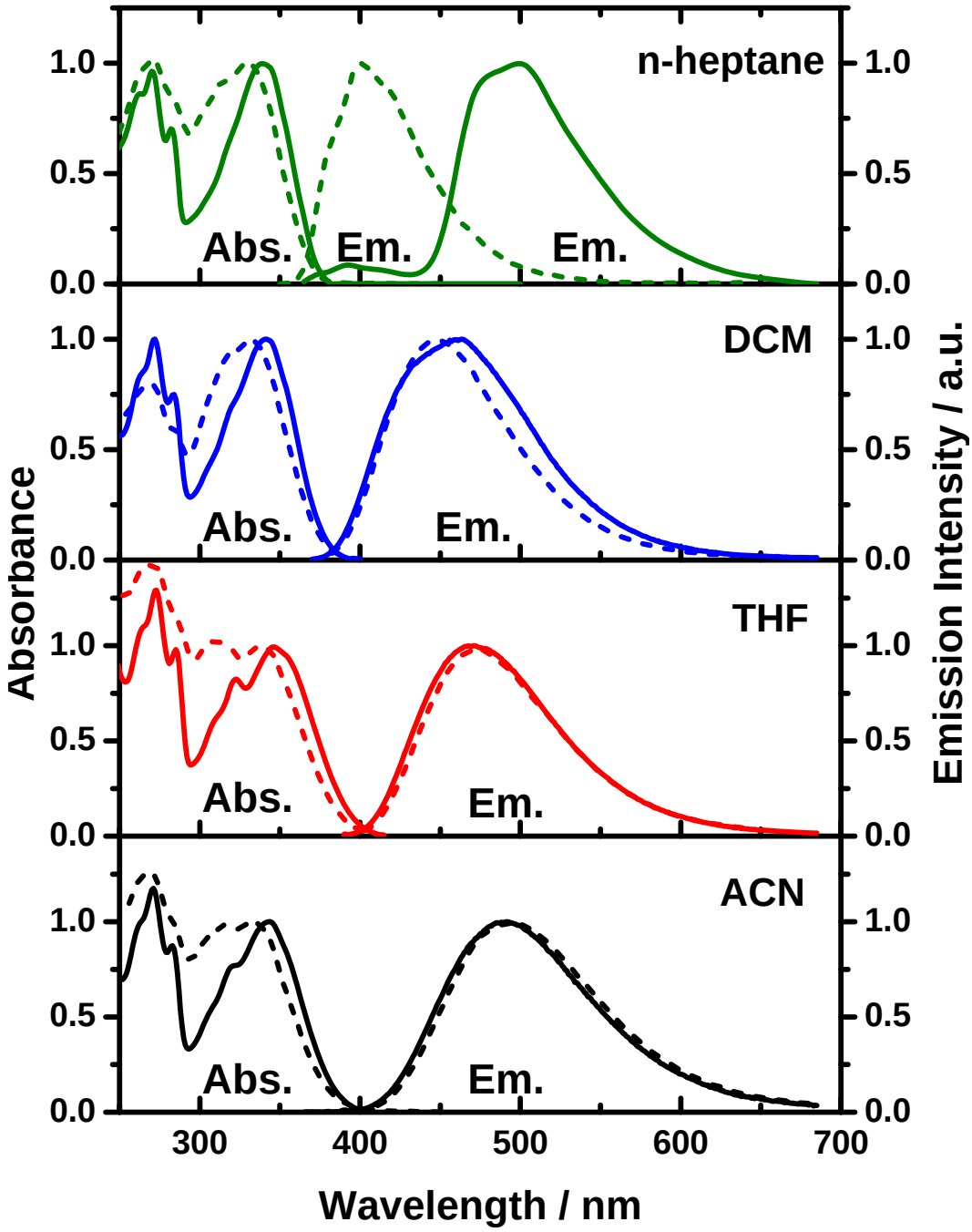

Figure 4.

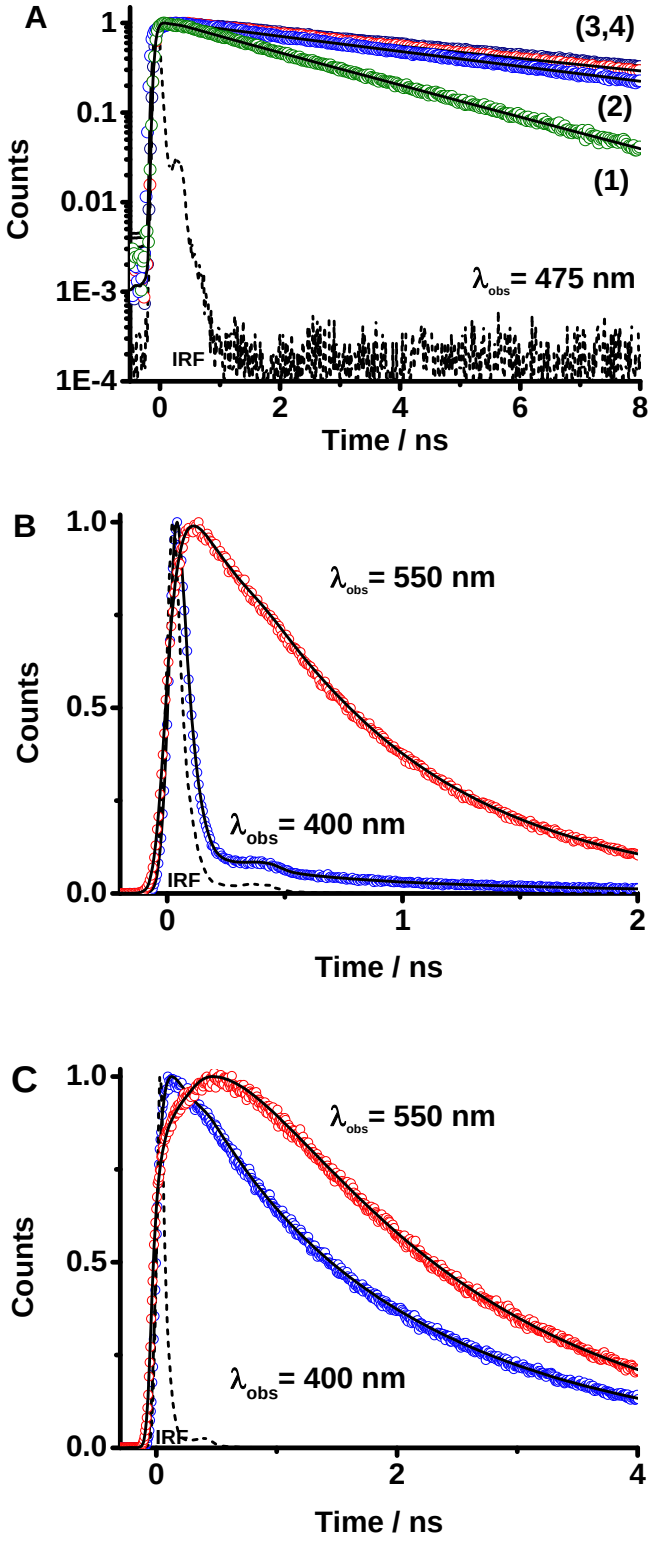

Figure 5.

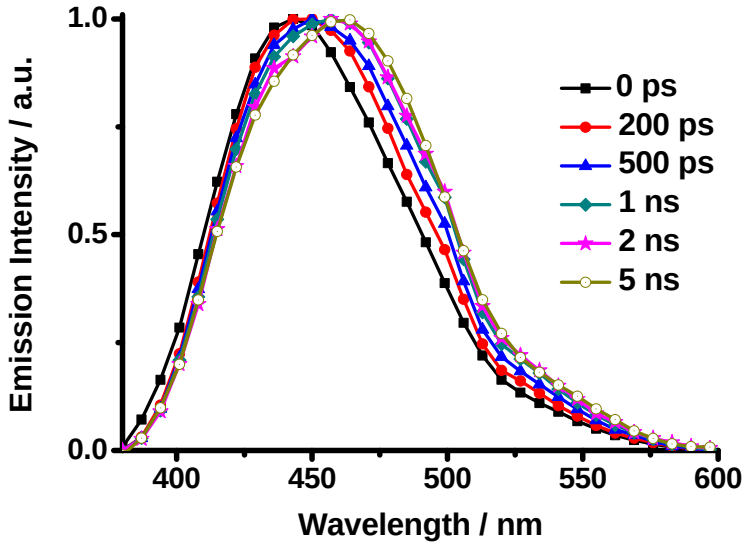

Figure 6.

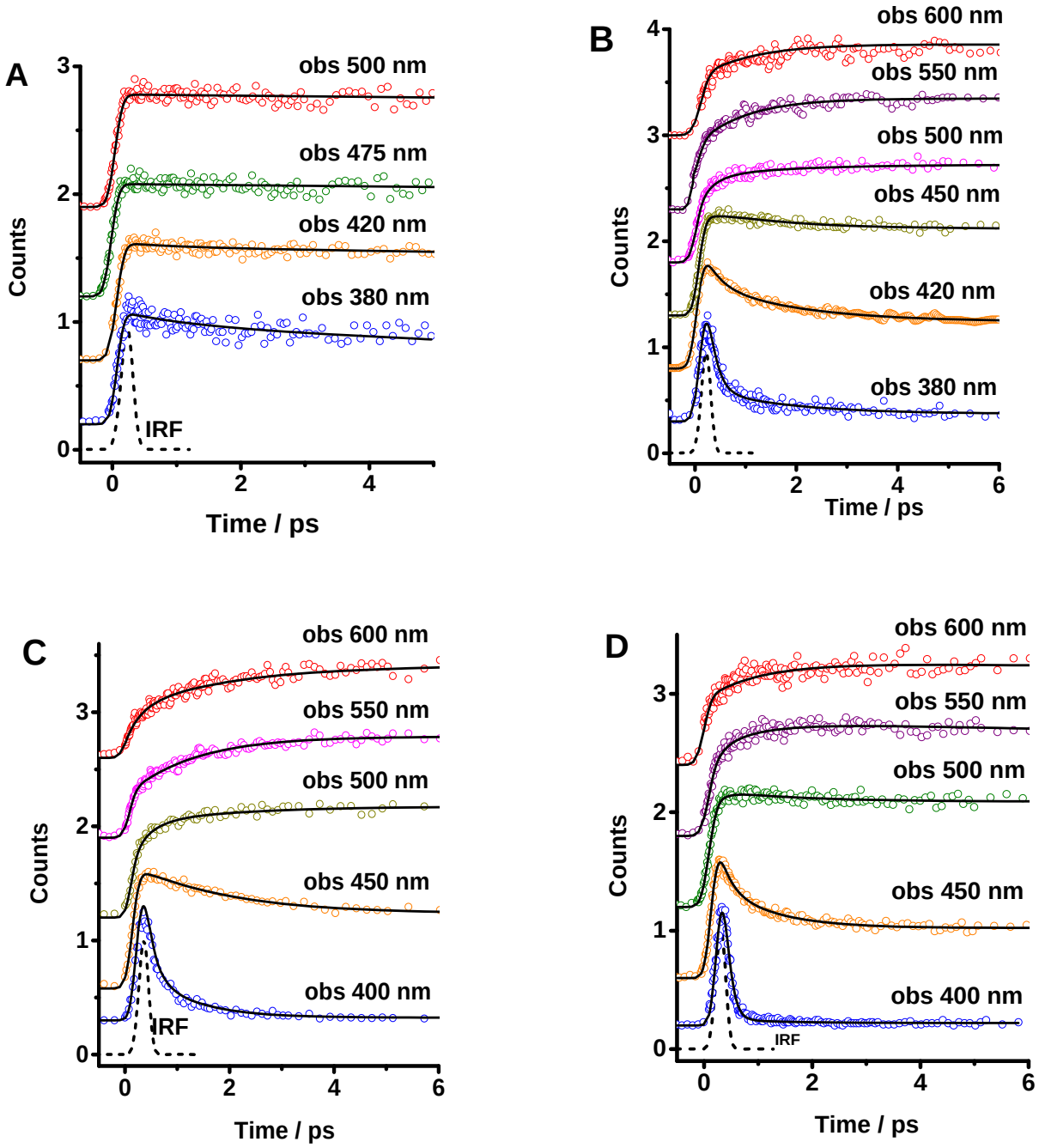

Figure 7

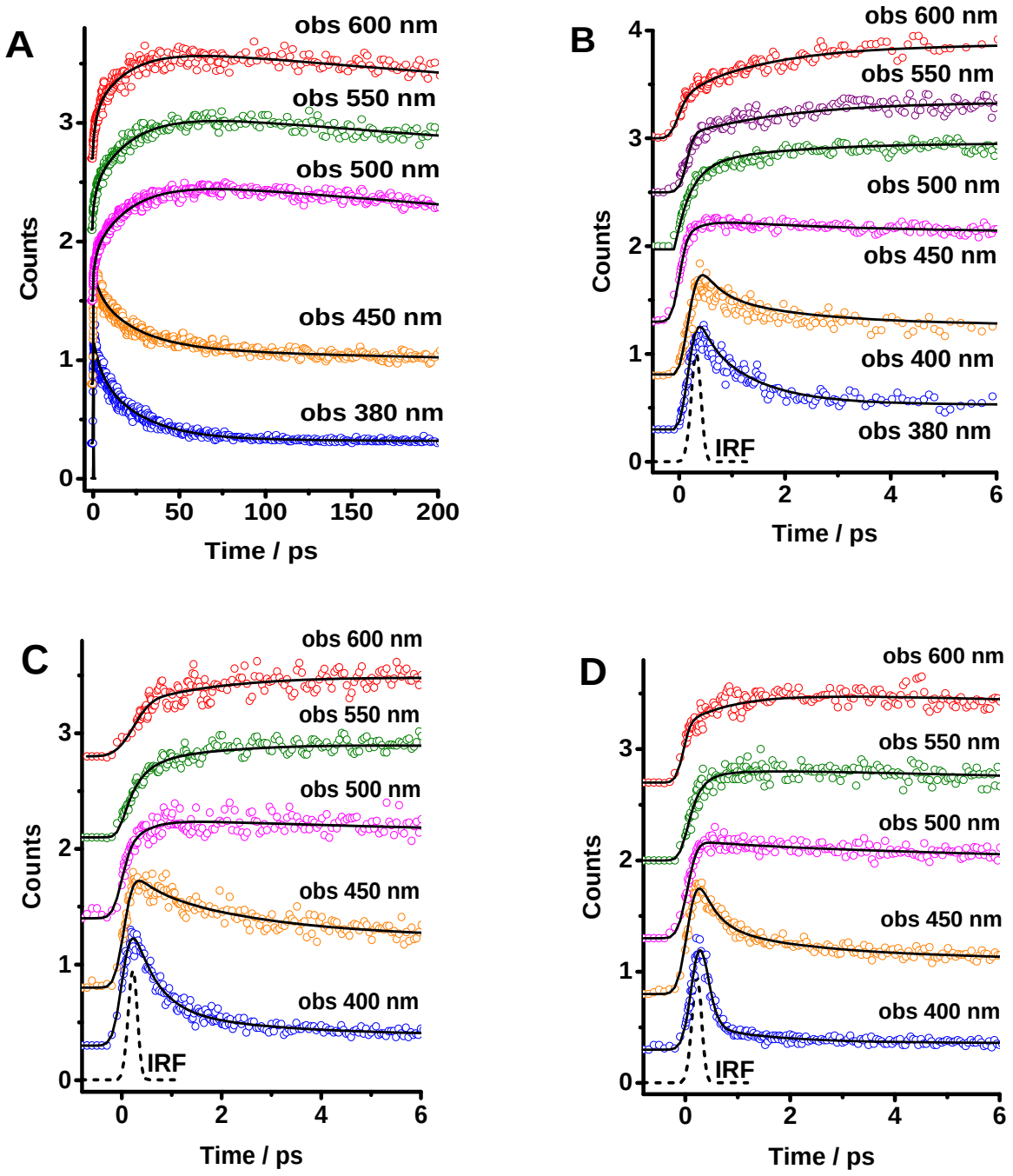

Table 1.

A)

	E at S_0	**E* (FC) at S_1**	**Relaxed E* at S_1**	**K* at S_1**
HBO	0.080	0.207	0.198	-0.392
5A-HBO	0.070	0.085	-0.003	-0.404

B)

Δμ/D	**E at S_0 → E* (FC) at S_1**	**E* (FC) at S_1→ Relaxed E* at S_1**	**Relaxed E* at S_1 → K* at S_1**
HBO	2.2	0.38	2.8
5A-HBO	1.8	3.7	4.1

Table 2.

Solvent	**λ_{Obs} /nm**	**τ_1 / ns** (± 0.2)	**A_1**	**a_1 %**	**c_1 %**	**τ_2 / ps** (± 50)	**A_2**	**a_2 %**	**c_2 %**	**τ_3 / ps** (± 5)	**A_3**	**a_3 %**	**c_3 %**
n-heptane	400	2.5	622	1	56	–	–	–	–	20	61200	99	44
	425	2.5	593	1	48	810	699	1	15	20	55370	98	37
	450	2.5	240	1	19	810	6700	11	67	22	35960	88	14
	475	–	–	–	–	810	11874	100	100	18	-16540	−100	−100
	500	–	–	–	–	810	12820	100	100	20	-17620	−100	−100
	550	–	–	–	–	810	12930	100	100	20	-18005	−100	−100
DCM	400	2.0	9640	77	93	500	2920	23	7	–	–	–	–
	450	2.0	10809	92	98	500	920	8	2	–	–	–	–
	475	2.0	13652	100	100	500	-2783	-100	-100	–	–	–	–
	550	2.0	15500	100	100	500	-7390	-100	-100	–	–	–	–
	650	2.0	8700	100	100	500	-8100	-100	-100	–	–	–	–

Table 3.

5A-HBO in DCM	
τ_1 / ns	2.0
τ_2 / ps	500
$A = A_{12}/A_{11}$	0.3
τ (ECT) / ns	5.0
τ (K) / ps	0.95
k_{DPT} / 10^8 s^{-1}	6.4
k_{RPT} / 10^8 s^{-1}	6.1
$K(k_{DPT}/k_{RPT})$	1.05
τ_{DPT} / ns	1.55
τ_{RPT} / ns	1.60
φ (ECT) (*)	0.14
φ (K) (*)	0.06
k_r (ECT) / 10^7 s^{-1}	8.5
k_{nr} (ECT) / 10^8 s^{-1}	1.7
k_r (K) / 10^7 s^{-1}	9.4
k_{nr} (K) / 10^8 s^{-1}	9.9

(*) Values obtained from a deconvolution of the dual emission spectrum.

Estimated Errors*:* τ (single exp.): 10%; τ (double exp.): 20%; φ: 20%; k_r and k_{nr}**:** 20%

Table 4.

Solvent	λ_{Obs}/nm	τ_1 / fs (± 50)	a_1%	τ_2 / ps (± 0.1)	a_2%	τ_3* / ns	a_3%
n-heptane	380	□	□	1.1	11	2.4	89
	420	□	□	1.1	14	2.4	86
	475	□	□	□	□	2.4	100
DCM	380	220	85	1.2	11	5.0	4
	420	240	34	1.2	30	5.0	36
	450	□	□	1.2	18	5.0	82
	500	□	□	1.2	□100	5.0	100
	550	□	□	1.2	□100	5.0	100
	600	□	□	1.2	□100	5.0	100
THF	400	280	77	1.2	22	6.2	1
	450	300	17	1.2	40	6.2	60
	500	□	□	1.2	□100	6.2	100
	550	□	□	1.2	□100	6.2	100
	600	□	□	1.2	□100	6.2	100
ACN	400	200	95	0.7	3	6.8	2
	450	200	40	0.7	29	6.8	31
	500	□	□	0.7	10	6.8	90
	550	□	□	0.7	□100	6.8	100
	600	□	□	0.7	□100	6.8	100

*Fixed values in the fit taking into account the TCSPC experiments.

Table 5.

Solvent	λ_{Obs}/nm	τ_1 / ps (± 0.05)	a_1%	τ_2 / ps (± 5)	a_2%	τ_3* / ns	a_3%
n-heptane	380	1.1	13	20	82	2.5	5
	450	1.1	8	20	59	2.5	33
	500	□	□	20	□78	0.8	100
	550	□	□	20	□80	0.8	100
	600	□	□	20	□82	0.8	100
DCM	380	0.3	64	1.2	23	2.0	13
	400	0.3	48	1.2	35	2.0	17
	450	□	□	1.2	19	2.0	81
	500	□	□	1.2	□100	2.0	100
	550	□	□	1.2	□100	2.0	100
	600	□	□	1.2	□100	2.0	100
THF	400	0.3	66	1.2	29	7.2	5
	450	0.3	10	1.2	22	7.2	68
	500	□	□	1.2	□100	7.2	100
	550	□	□	1.2	□100	7.2	100
	600	□	□	1.2	□100	7.2	100
ACN	400	0.2	92	0.6	5	6.7	3
	450	0.2	43	0.6	30	6.7	27
	500	□	□	0.6	11	6.7	89
	550	□	□	0.6	□100	6.7	100
	600	□	□	0.6	□100	6.7	100

*Fixed values in the fit taking into account the TCSPC experiments.